Diffusion Imaging with Hyperpolarized ^{3}He

D. M. Schmidt, J. S. George (P-21), S. I. Penttila (P-23), A. Caprihan, E. Fukushima (Lovelace Respiratory Research Institute, Albuquerque, New Mexico)

Several novel aspects of nuclear magnetic resonance (NMR) or magnetic resonance imaging (MRI) with hyperpolarized noble gases have recently been demonstrated, including the ability to easily image gas-filled spaces[1,2] and to transfer part of the polarization to other nuclei.[3,4] Using these new techniques, we have been investigating diffusion. We obtained one-dimensional images of ^{3}He gas diffusing in a slice that was tagged by inverting its magnetization, a technique previously used for observing the diffusion of thermally polarized ^{129}Xe gas.[5] Also, a one-dimensional diffusion image of the gas was made with and without a temperature gradient present. Our results show that temperature changes can be monitored by diffusion images of ^{3}He gas.

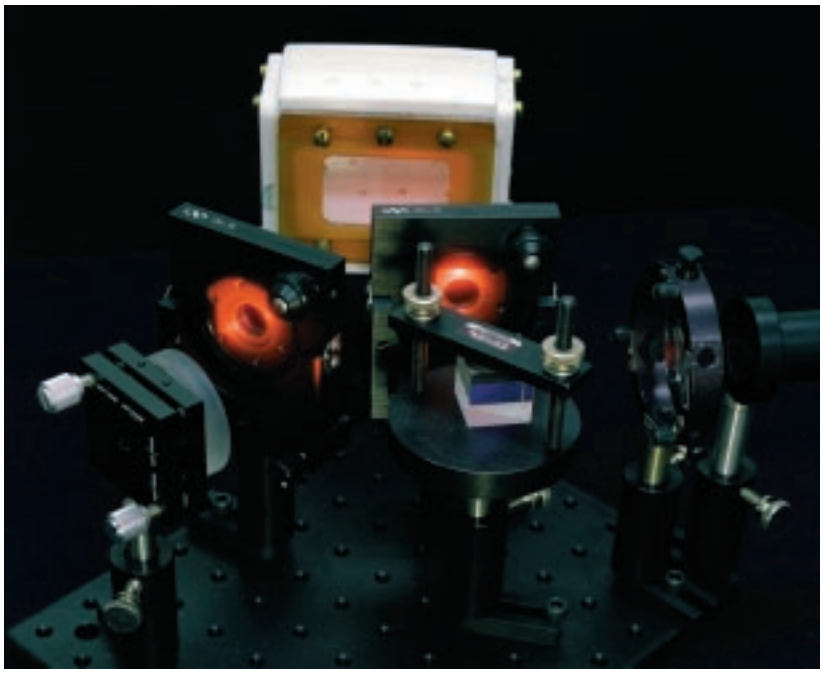

Fig. II-1. A photograph of the portable apparatus used to polarize the ^{3}He gas.

The experiments were performed in an NMR imager/spectrometer at the Lovelace Respiratory Research Institute in Albuquerque, New Mexico. Rather than thermally polarizing the ^{3}He gas in the magnetic field of the imaging magnet, we hyperpolarized the gas externally with a laser. In this technique, rubidium atoms are first polarized with circularly polarized laser light, which then polarizes the ^{3}He gas through spin-exchange collisions.[6,7] The ^{3}He gas was at 7 atm of pressure in a cylindrical glass cell with an inner length of 7.0 cm and an inner diameter of 2.2 cm. Figure II-1 shows the polarizing apparatus. For each set of images, the gas was polarized in the fringe field of the 1.9-T imaging magnet at a distance of 2 m for a few hours using a 15-W diode-laser array.[8] The polarization time constant of the cell (T1) was about 15 h, and with 4 h of optical pumping, a polarization of about 5% was achieved. This polarization is over three orders of magnitude larger than the polarization that would be obtained with conventional thermal polarization, and thus it significantly improves our ability to image the gas. A two-dimensional projection image of the hyperpolarized gas is shown in Fig. II-2.

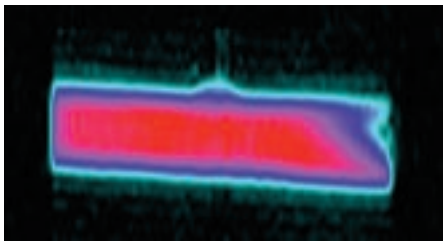

Fig. II-2. A two-dimensional projection image of the hyperpolarized ^{3}He gas in its cylindrical cell. The 1-mm stem that is used for filling the cell is visible in the top-center portion of the image.

A series of one-dimensional images over time were obtained in which the diffusion of two populations of nuclei could be seen in a manner similar to that in Ref. 5. First, the magnetization of the nuclei in a thin, central section of the cylinder was inverted. Then, images were taken every 0.2 s for a total of 5 s, using a constant flip angle of 4.5°. Because the gas had such a long T1, the fraction of the magnetization (sin[4.5°]) that was lost due to dephasing with each image acquisition did not recover over the 5-s duration of the experiment. The series of images, normalized to the same total intensity, are shown in Fig. II-3.

The ^{3}He diffusion coefficient was determined with this data using a simple model. A delta-function spike in density will, through diffusion, form a density profile that is Gaussian, with a variance proportional to the diffusion coefficient and to the time over which diffusion has taken place.[9] We therefore modeled each one-dimensional image by convolving the first image with a Gaussian distribution whose variance V was proportional to a diffusion coefficient D times the time interval t separating the two images: $V = 2Dt$. We then searched for the value of D that minimized the error between the predicted and measured values using a chi-squared statistic. This model does not account for the cell walls, so only the pixels that were sufficiently far away from the walls were used in the fit. In addition, to correct for the decreasing signal, we first normalized each image to the same total signal intensity. A comparison of the experimental data to the model with the best-fitting value of D is shown in Fig. II-4 for a few selected time intervals. A value of $D = (12.3 \pm 0.2)$ mm^2/s was obtained.

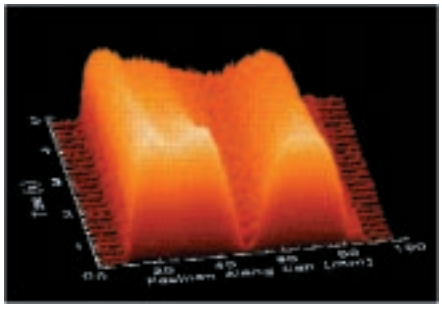

Fig. II-3. A series of one-dimensional images of the gas over time, showing the diffusion of the small central slice of inverted magnetization. Time runs from front to back, with the total duration being 5 s.

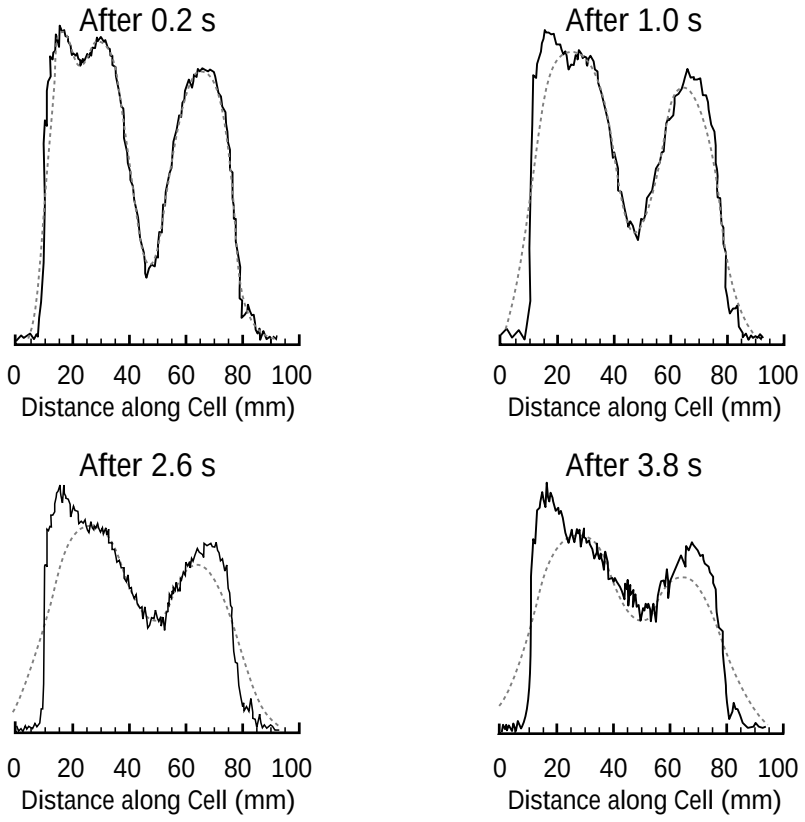

Fig. II-4. A comparison of the data (solid) and model (dashed) for a few selected time intervals using the best-fit value of the diffusion coefficient. The model does not take into account the cell boundaries; the pixels included in the fit are only those that are far enough away from the boundaries to remain unaffected by them.

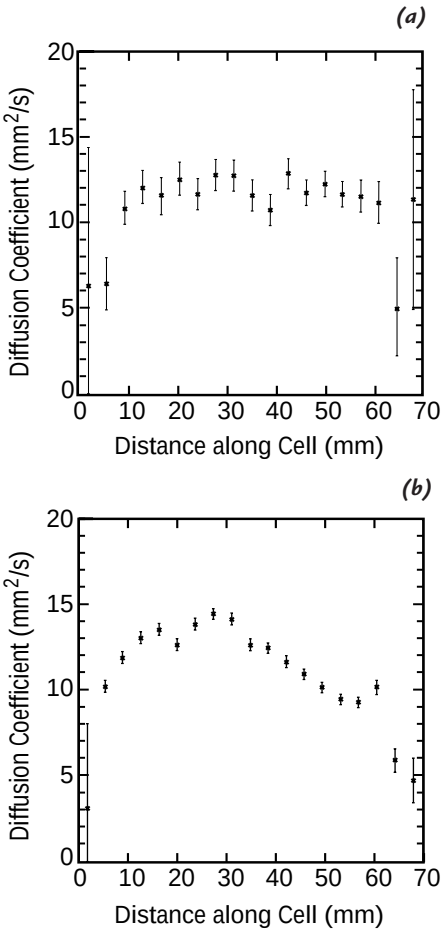

Fig. II-5. Two diffusion images (a) without and (b) with a thermal gradient in place. The reduction in the diffusion coefficient near the cell boundaries in both images is due to restricted diffusion. The decrease in diffusion from left to right in the lower image reflects the decrease in temperature from left to right.

Next, one-dimensional diffusion images were made using the technique of Stejskal and Tanner.[10] A diffusion coefficient was calculated at each point in the image by taking the ratio of the image intensities with and without a previous magnetic-field gradient in place. With a gradient, the signal will diminish because of diffusion. Knowing the strength and duration of the gradient allows the diffusion coefficient to be determined.

Diffusion can be affected by physical boundaries as well as by temperature or pressure. Images were made both at thermal equilibrium and with a thermal gradient (Fig. II-5). The value of every fifth pixel averaged with its four nearest neighbors is shown in these images. In the upper plot in Fig. II-5, the gas is at thermal equilibrium at room temperature. Error bars in this plot are larger than those in the lower plot because the data for the upper plot were acquired after a shorter polarization time and therefore had smaller signals. The diffusion coefficient away from the ends of the cylinder is consistent with that measured from observing the diffusion of a section of inverted magnetization (described above). The lowering of the diffusion coefficient near the walls of the cylinder is due to the walls restricting the diffusion in this area and is the cause of the edge enhancements discussed in Ref. 11. The lower plot shows a diffusion image when the cylinder had a thermal gradient produced by holding the right end (as viewed in this figure) of the cell in a liquid-nitrogen exhaust plume for a few minutes. The diffusion coefficient decreases with temperature. Again, lowering of the diffusion coefficient at the ends is due to restricted diffusion.

We have demonstrated the use of diffusion imaging with a hyperpolarized noble gas for monitoring temperature and for detecting physical boundaries. Just like relaxation-time images, spatial maps of diffusion can be a useful technique for characterizing the environment of the molecules containing the nuclei being imaged. We believe that diffusion imaging of hyperpolarized noble gases offers unique advantages in characterizing the porosity of materials, studying fractures in rocks, and dynamically imaging the pressure and temperature distributions in biological and acoustical systems.

References

1. M. S. Albert, G. D. Cates, B. Driehuys, et al., "Biological Magnetic Resonance Imaging Using Laser-Polarized ^{129}Xe," *Nature* **370**, 199 (1994).

2. H. Middleton, R. D. Black, B. Saam, et al., "MR Imaging with Hyperpolarized ^{3}He Gas," *Magnetic Resonance in Medicine* **33**, 271 (1995).

3. C. R. Bowers, H. W. Long, T. Pietrass, et al., "Cross Polarization from Laser-Polarized Solid Xenon to $^{13}CO_2$ by Low-Field Thermal Mixing," *Chemical Physics Letters* **205**, 168 (1993).

4. G. Navon, Y.-Q. Song, T. Rõõm, et al., "Enhancement of Solution NMR and MRI with Laser-Polarized Xenon," *Science* **271**, 1848 (1996).

5. M. Pfeffer and O. Lutz, "Observation of Diffusion in Xenon Gas by NMR," *Journal of Magnetic Resonance A* **113**, 108 (1995).

6. N. D. Bhaskar, W. Happer, and T. McClelland, "Efficiency of Spin Exchange between Rubidium Spins and ^{129}Xe Nuclei in a Gas," *Physical Review Letters* **49**, 25 (1982).

7. W. Happer, E. Miron, S. Schaefer, et al., "Polarization of the Nuclear Spins of Noble-Gas Atoms by Spin Exchange with Optically Pumped Alkali-Metal Atoms," *Physical Review A* **29**, 3092 (1984).

8. W. Cummings, O. Häusser, W. Lorenzon, et al., "Optical Pumping of Rb Vapor Using High-Power $Ga_{1-x}Al_xAs$ Diode Laser Arrays," *Physical Review A* **51**, 4842 (1995).

9. E. L. Cussler, *Diffusion: Mass Transfer in Fluid Systems* (Cambridge University Press, New York, 1984), p. 40.

10. E. O. Stejskal and J. E. Tanner, "Spin Diffusion Measurements: Spin Echoes in the Presence of a Time-Dependent Field Gradient," *Journal of Chemical Physics* **42**, 288 (1965).

11. P. T. Callaghan, A. Coy, et al., "Diffusive Relaxation and Edge Enhancement in NMR Microscopy," *Journal of Magnetic Resonance A* **101**, 347 (1993).